

The WIMP Forest: Indirect Detection of a Chiral Square

Gianfranco Bertone^a, C. B. Jackson^b, Gabe Shaughnessy^{b,c}, Tim M.P. Tait^{b,c}, Alberto Vallinotto^d

^a *Institut d'Astrophysique de Paris, France. UMR7095-CNRS
Université Pierre et Marie Curie, 98bis Boulevard Arago, 75014 Paris, France*

^b *Argonne National Laboratory, Argonne, IL 60439*

^c *Northwestern University, 2145 Sheridan Road, Evanston, IL 60208 and*

^d *Center for Particle Astrophysics, Fermi National Accelerator Laboratory,
P.O. Box 500, Kirk Rd. & Pine St., Batavia, IL 60510-0500 USA*

(Dated: May 28, 2018)

The spectrum of photons arising from WIMP annihilation carries a detailed imprint of the structure of the dark sector. In particular, loop-level annihilations into a photon and another boson can in principle lead to a series of lines (a WIMP forest) at energies up to the WIMP mass. A specific model which illustrates this feature nicely is a theory of two universal extra dimensions compactified on a chiral square. Aside from the continuum emission, which is a generic prediction of most dark matter candidates, we find a “forest” of prominent annihilation lines that, after convolution with the angular resolution of current experiments, leads to a distinctive (2-bump plus continuum) spectrum, which may be visible in the near future with the Fermi Gamma-Ray Space Telescope (formerly known as GLAST).

I. INTRODUCTION

Cosmological and astrophysical observations provide compelling evidence for dark matter (DM), but so far they have not provided a smoking-gun indication of its identity. The hunt for dark matter is now entering a new era, with the current generation of indirect and direct detection experiments closing in on weak scale masses and couplings, and the LHC turn-on just around the corner. Among the plethora of dark matter candidates, Weakly Interacting Massive Particles (WIMPs) appear particularly appealing, since they combine the virtues of weak scale masses and couplings, stability, and connection to the mystery of electroweak symmetry-breaking [1].

If WIMPs do indeed have weak scale masses and interactions, they are expected to produce observable effects in colliders and astroparticle experiments. In particular, indirect detection experiments seek secondary particles produced by the annihilation of WIMPs in regions of our galaxy where the DM density is high, e.g. the Galactic center, or DM clumps. Among secondary particles, gamma-rays play a special role, since they have the advantage of traveling in straight lines and without sizable energy losses in the local universe, thus tracing the distribution of DM in a straightforward way.

The annihilation of WIMPs into photons typically proceeds via a complicated set of processes, and the final spectrum actually contains a detailed imprint of WIMP annihilation that can in principle reveal features such as the WIMP spin and/or other particles in the dark sector. Tree-level anni-

hilation of WIMPs into quarks or leptons (or heavier states which decay into them) provides a continuum of photon energies, with an upper cutoff at approximately the WIMP mass. This continuum emission is in general rather featureless, but some models do exhibit spectacular features, such as a high-energy rise due to final state radiation [2]. Furthermore, loop-level annihilation into a photon and X results in a line at energy

$$E_\gamma = m_{DM} \left(1 - \frac{M_X^2}{4m_{DM}^2} \right), \quad (1)$$

where m_{DM} is the WIMP mass and M_X the mass of the other boson in the final state (in supersymmetric theories, X is either another photon or a Z boson [3]). Line emission typically has smaller magnitude than continuum emission, but the line provides a feature that helps discriminate against backgrounds. More generally, it may also be that the tree-level annihilation is into photon-unfriendly modes, and the line(s) may turn out to be prominent features in the photon energy spectrum.

At energies in the 10 GeV – 10 TeV range, the energy resolution of current gamma-ray telescopes such as the Fermi LAT or Air Cherenkov Telescopes like CANGAROO, HESS, MAGIC and VERITAS, is of order $\Delta E/E \sim 0.1$. When the mass of X is small compared to the WIMP mass, different lines may merge together because of finite detector resolutions. When X has a mass which is appreciable compared to the WIMP mass, the lines can be distinct and separately measurable. When distinct, they provide information about physics beyond the Standard Model. For example, the position of the $\gamma\gamma$ line measures the WIMP mass.

The relative strengths of the $\gamma\gamma$ and γZ lines are a measure of the WIMP coupling to $SU(2)$ singlets versus doublets. An unsuppressed γH line (where H is a Higgs boson) would be an indication that the WIMP is not a Majorana fermion or a scalar. Finally, if there are particles in the dark sector whose mass is less than $2m_{DM}$, then a pair of WIMPs may be able to annihilate into one of these exotic heavy states and a photon. The existence of such a line could be the first indication that such a heavy partner is present. Taken all together, there could be a “forest” of lines associated with WIMP annihilations, and they represent a wealth of information about the theory of dark matter.

A specific model which illustrates these features nicely is the “Chiral Square” [4], a six dimensional model with universal extra dimensions (UED) [5] – extra dimensions in which the entire Standard Model (SM) propagates. UED theories contain WIMP candidates because of remnants of the extra-dimensional spacetime symmetries which forbid the lightest of the Kaluza-Klein excitations of the SM from decaying. The Chiral Square is an intrinsically six dimensional construction, whose dark matter candidate, the “spinless photon” [6] (the KK mode of the hypercharge vector boson whose spin is pointing in the extra dimension) has distinct phenomenology compared to the five dimensional case [7, 8, 9, 10]. Six dimensional implementations of the SM have a mechanism which automatically suppresses dangerous higher dimensional operators leading to proton decay [11] and motivate the existence of three generations of fermions through gauge anomaly cancellation [12].

The article is laid out as follows. In Section II we (briefly) review the chiral square model, and what is currently known about its dark matter candidate. In Section III, we calculate the continuum gamma ray spectrum from WIMP annihilations in the galaxy. Section IV outlines the calculation of the cross sections for the annihilation processes of two WIMPs into states with one or two final primary photons. In Section V we discuss the prospects for detection of the astrophysical signal and the related uncertainties. We finally reserve Section VI for the conclusions.

II. THE CHIRAL SQUARE

The chiral square is a model of two compact universal extra dimensions. The extra dimensional coordinates may be represented by a pair of points (x^5, x^6) living in a square region with sides L . Ad-

jacent sides of the square are identified with each other,

$$(y, 0) \equiv (0, y) \quad (y, L) \equiv (L, y) \quad (2)$$

which is equivalent to taking a square, folding it along a diagonal, and smoothly gluing the edges together. The folding leaves the two corners of the square which lie along the fold (at $(0, 0)$ and (L, L)) invariant, and identifies the remaining two corners (at $(0, L)$ and $(L, 0)$) as the same point.

The Kaluza Klein (KK) modes of SM fields are labelled by a pair of integers, (j, k) which satisfy,

$$k \geq 0 \quad , \quad j \geq 1 - \delta_{k,0} \quad . \quad (3)$$

Scalar fields have wave functions,

$$f^{(j,k)}(x^5, x^6) = \frac{1}{L}(C_+ + C_-), \quad (4)$$

$$C_{\pm} = \cos \pi \left(\frac{jx^5 \pm kx^6}{L} \right),$$

with masses given (up to boundary term effects described below) by,

$$M_{(j,k)}^2 = M_0^2 + \pi^2 \frac{j^2 + k^2}{L^2}, \quad (5)$$

where M_0^2 is the mass of the “zero-mode” field, which carries no momentum in the extra dimensional directions, and has wave function $f^{(0,0)} = 1/(2L)$. We identify the zero modes with the Standard Model fields.

The KK modes of fermions are Dirac particles. The (4D) chirality associated with the zero mode works essentially as outlined above, but the opposite chirality pieces have wave functions which are phase-shifted. The full details are presented in [4], and are not essential for our purposes. The gauge bosons V^M decompose into 4D vectors V^μ and two 4D scalars, V^5 and V^6 . One linear combination of V^5 and V^6 is eaten, level by level, by the vector KK modes to provide their longitudinal degrees of freedom. The other linear combination of V^5 and V^6 are physical gauge adjoint scalars in the 4D effective theory. We follow the usual convention and denote them by $V_H^{(j,k)}$.

The residual space-time symmetry causes the lightest $(1, 0)$ KK particle (LKP) to be stable. The allowed “large” interactions can be roughly understood from higher dimensional momentum conservation, but with the important observation that since moving across a boundary rotates the direction of the momentum by 90° , the momentum in the x^5 and x^6 directions are not actually distinct from one another. The full momentum

conservation, even in this folded sense, is broken by terms which live on the corners of the square [13] (and whose presence is required when the theory is renormalized [14, 15]), which nevertheless preserve a bulk symmetry (invariance under reflections through the middle of the square), provided the UV physics is such that equal boundary terms live at $(0,0)$ and (L,L) . Even in the presence of such terms, there is a Z_2 KK-parity [4] under which states that have $j+k$ equal to an even integer are even, and states with $j+k$ odd are odd. Just as in the 5D case [15, 16] the boundary terms have the effect of breaking degeneracies within a given KK level and introducing KK-number violating (but KK-parity preserving) couplings among the KK modes [13].

We follow the usual reasoning, and assume that the boundary terms are dominated by radiative contributions from the bulk physics [15]. While not strictly required by any theoretical or phenomenological argument,¹ loop-level boundary terms motivate having the colored and charged KK modes being heavier than their neutral counterparts (which, at least at the $(1,0)$ level is essential for the theory to contain a viable WIMP).

Motivated by the expectations of radiative boundary terms, the lightest $(1,0)$ mode is expected to be the scalar partner of the hypercharge boson, $B_H^{(1,0)}$ (which we will often abbreviate as simply B_H) [13]. While electroweak symmetry-breaking mixes $B_H^{(1,0)}$ with its $SU(2)$ counterpart, $W_H^{(1,0)}$, the mixing angle is typically small, and the LKP is, to good approximation, pure B_H . This implies that the LKP is a gauge singlet, whose coupling to SM fermions and Higgs is controlled by the $U(1)$ gauge coupling g_1 and the hypercharge of the matter field. As a further consequence of small boundary terms, its largest couplings are expected to be those which are KK number conserving (in the folded sense above).

The LKP, as a real scalar, has a suppressed annihilation rate to light fermions in the present epoch and therefore annihilates predominantly into pairs of electroweak bosons WW and ZZ , Higgs bosons HH , and (if heavy enough) pairs of top quarks $t\bar{t}$ [6]. As a result, its thermal relic density is very sensitive to its mass and the mass of the zero mode Higgs, which provides a resonant annihilation channel when $M_H \sim 2m_{B_H}$. The relic density

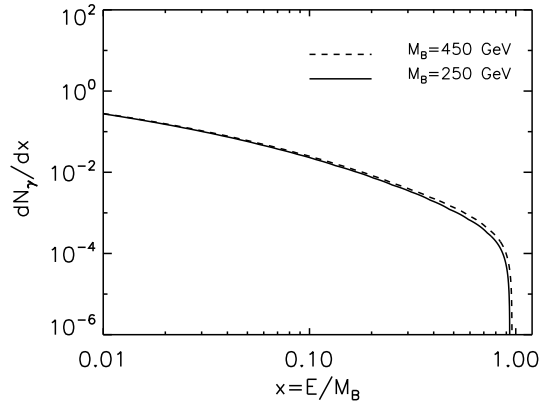


FIG. 1: Continuum photon spectra, dN_γ/dx for two mass choices of B_H .

is consistent for masses in the range of roughly 200-500 GeV, with narrow windows of Higgs masses appropriate for each LKP mass. We use the relic density as a rough guideline to the most interesting range of LKP masses for indirect detection, but do not strictly assume it applies; it could be that the LKP is not a thermal relic, or our extrapolation of cosmology to early times is flawed by imperfect understanding.

III. CONTINUUM γ -RAY EMISSION

As mentioned above, pairs of LKPs annihilate predominantly into pairs of electroweak bosons WW and ZZ , Higgs bosons HH , and (if heavy enough) pairs of top quarks $t\bar{t}$. Far above the $t\bar{t}$ and HH thresholds, the annihilation fractions are roughly 50% $B_H B_H \rightarrow WW$, 25% $B_H B_H \rightarrow ZZ$, 25% $B_H B_H \rightarrow HH$, with $B_H B_H \rightarrow t\bar{t}$ subdominant. Continuum gamma ray emission is largely the result of radiation from charged leptons which result when these massive objects decay, or decays of π^0 s from the hadronization of strongly interacting decay products. The result is a rather soft spectrum of gamma rays, reminiscent of neutralinos in supersymmetric models.

We compute the continuum spectrum using the micrOMEGAs code [18], based on a CalcHEP [19] (partial) implementation of the chiral square model [20]. From Fig. 1, where the differential flux (per steradian) from the continuum spectrum is plotted for $M_{B_H} = 250$ GeV and for $M_{B_H} = 450$ GeV it is interesting to point out that the spectrum sharply decreases well before the value of

¹ However, analysis of large boundary terms in 5D does reveal that when they are large, it is generically more difficult to fit precision EW data [17].

M_{B_H} . This is a distinctive feature of this specific chiral square model and is related to the fact that the dominant annihilation channels are into photon unfriendly modes, consisting of massive (and often neutral) particles which are unlikely to radiate high energy photons. This leaves the bulk of the photons coming as radiation (or after hadronization, decays of π^0 s) from the even softer decay products of the particles produced in the primary annihilation, which have less energy available for the final state photons.

IV. CROSS SECTIONS FOR γ -RAY LINES

Let us now consider the direct annihilation of LKP pairs into photons. Specifically, we will consider the process $B_H B_H \rightarrow \gamma V$ where V can be either a photon, Z boson or a KK excitation of a SM gauge field. Since the LKP has no direct coupling to the photon, the leading-order contributions to these processes occur at one loop. Examples of Feynman diagrams are shown in Fig. 2. Here we assume that the dominant contributions are from loops of SM charged fermions (ℓ) and their corresponding pairs of KK partners ($\xi_{s,d}^{(\ell)}$). Note that, at a given KK level, the fermionic field content is doubled as compared to the SM such that each SM fermion has both a singlet ($\xi_s^{(\ell)}$) and doublet ($\xi_d^{(\ell)}$) KK partner.

The matrix element for the generic process $B_H(p_1)B_H(p_2) \rightarrow \gamma^\mu(p_A)V^\nu(p_B)$ takes the form:

$$\mathcal{M} = \epsilon_A^{\mu*}(p_A)\epsilon_B^{\nu*}(p_B)\mathcal{M}^{\mu\nu}(p_1, p_2, p_A, p_B), \quad (6)$$

where ϵ_A^μ and ϵ_B^ν are the polarization tensors of the photon and V gauge boson, respectively.

In general, the amplitude $\mathcal{M}^{\mu\nu}$ can be expressed as a linear combination of tensor structures built from the external momenta and the metric tensor

$g^{\mu\nu}$. Considering the transversality of the polarization tensors, $\epsilon_A \cdot p_A = \epsilon_B \cdot p_B = 0$, the most general tensor structure is given by:

$$\begin{aligned} \mathcal{M}^{\mu\nu} = & A_1 g^{\mu\nu} + B_1 p_1^\mu p_1^\nu + B_2 p_2^\mu p_2^\nu + B_3 p_1^\mu p_2^\nu \\ & + B_4 p_1^\nu p_2^\mu + B_5 p_A^\nu p_B^\mu + B_6 p_1^\mu p_A^\nu + B_7 p_1^\nu p_B^\mu \\ & + B_8 p_2^\mu p_A^\nu + B_9 p_2^\nu p_B^\mu. \end{aligned}$$

However, WIMPs are assumed to be highly non-relativistic (with typical velocities of $v \sim 10^{-3}$), such that the incoming momenta of the B_H 's are well approximated by $p_1 = p_2 \equiv p$ where $p = (m_{B_H}, \mathbf{0})$. Thus, using conservation of momentum ($2p^\mu = p_A^\mu + p_B^\mu$), we can eliminate many of the above terms. In addition, since the WIMP's are annihilating nearly at rest, the final state products are emitted back-to-back such that (to a good approximation):

$$\epsilon_A \cdot p_B = \epsilon_B \cdot p_A = 0. \quad (7)$$

Finally, dot products of the form $\epsilon_{A,B} \cdot p$ will be velocity-suppressed and can be safely neglected. Thus, of the ten original tensor structures which make up $\mathcal{M}^{\mu\nu}$, only the $g^{\mu\nu}$ term survives. We have explicitly checked that, indeed, the A_1 term is the dominant contribution even when all of the tensor structures are kept.

In the calculation of the loop amplitudes, we apply the following algorithm. First, we reduce all dot products of the form $k \cdot p$ (where k is the loop momentum and p is a generic external momentum) against the corresponding factors from propagators in the denominator. The resulting three-point functions can be safely computed using the standard Passarino-Veltman (PV) technique [21]. The remaining terms in the amplitudes take the form of four-point scalar (D_0) and rank-two tensor ($D_{\mu\nu}$) functions:

$$D_{0;\mu\nu}(p_1, p_2, p_3; m_1, m_2, m_3, m_4) = \int \frac{d^n k}{i\pi^2} \frac{\{1; k_\mu k_\nu\}}{[k^2 - m_1^2][(k + p_1)^2 - m_2^2][(k + p_1 + p_2)^2 - m_3^2][(k + p_1 + p_2 + p_3)^2 - m_4^2]}, \quad (8)$$

where p_i are external momenta and m_i are the masses of the particles circling the loops. Note that we have neglected rank-one tensor integrals (D_μ) since we are only interested in extracting the $g_{\mu\nu}$ pieces of the amplitude.

Following the PV scheme, the rank-two tensor integral can be rewritten as a linear expansion in tensor structures which are built from the external

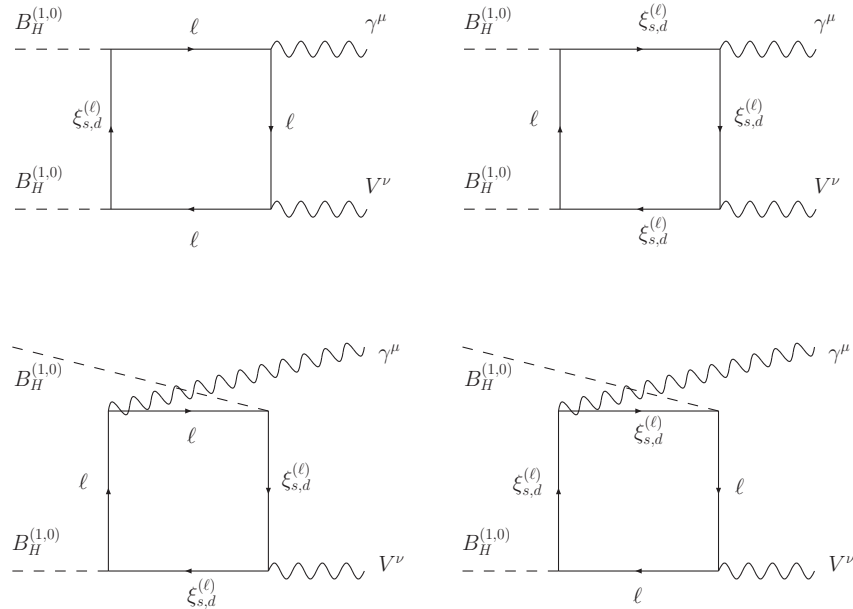


FIG. 2: Examples of Feynman diagrams which contribute to $B_H B_H \rightarrow \gamma V$ where $V = \gamma, Z$ and $B^{(1,1)}$.

momenta and the metric tensor:

$$D_{\mu\nu} = D_{21}p_{1,\mu}p_{2,\nu} + D_{22}p_{2,\mu}p_{2,\nu} + \dots + D_{27}g_{\mu\nu}, \quad (9)$$

The coefficients of this expansion (D_{ij}) can then be reduced to scalar integrals [21]. However, in cases where two of the external momenta become identical, as for the case of WIMP annihilation, this approach breaks down. In these cases, the expressions for the D_{ij} coefficients in terms of scalar integrals depend inversely on the Gram Determinant (GD) built from the external momenta (i.e., $\text{GD} = \det(p_i \cdot p_j)$). In certain kinematical regions (e.g., where two of the momenta become degenerate and $\text{GD} \simeq 0$), the PV scheme gives rise to spurious divergences. In calculations for collider processes (where the momenta are integrated over an entire phase space), this situation arises only at *special* points near the boundaries of phase space. Special techniques involving interpolating from these *unsafe* regions of phase space to *safe* regions have been developed to deal with these spurious divergences in calculations for collider processes.

These techniques do not apply to our situation (where the two incoming momenta are fixed *and* identical) and we are forced to approach this problem using the following method. For our calcula-

tion, we have chosen to implement the technique developed in Ref. [22]. In this algebraic reduction scheme, the original PV scheme is extended to deal with situations where the GD *exactly* vanishes. Higher-point tensor (and scalar) integrals are expressed in terms of lower-point quantities which can be safely evaluated utilizing the usual numerical techniques. For example, the expressions for the four-point scalar integral (D_0) and the tensor coefficient (D_{27}) can be expressed as:

$$D_0 = \alpha_{123}C_0(123) + \alpha_{124}C_0(124) + \alpha_{134}C_0(134) + \alpha_{234}C_0(234), \quad (10)$$

and:

$$D_{27} = \alpha_{123}C_{24}(123) + \alpha_{124}C_{24}(124) + \alpha_{134}C_{24}(134) + \alpha_{234}C_{24}(234), \quad (11)$$

where $C_0(ijk)$ and $C_{24}(ijk)$ are the three-point scalar integral and PV tensor coefficient, respectively (the (ijk) denotes various propagator factors in the original four-point denominator). The α_{ijk} coefficients can be obtained by solving the matrix equation:

$$\begin{pmatrix} 1 & 1 & 1 & 1 \\ 0 & p_1^2 & (p_1^2 - p_2^2 + p_5^2)/2 & (p_1^2 + p_4^2 - p_6^2)/2 \\ 0 & (-p_1^2 - p_2^2 + p_5^2)/2 & (-p_1^2 + p_2^2 + p_5^2)/2 & (-p_1^2 - p_3^2 + p_5^2 + p_6^2)/2 \\ -m_1^2 & p_1^2 - m_2^2 & p_5^2 - m_3^2 & p_4^2 - m_4^2 \end{pmatrix} \begin{pmatrix} \alpha_{234} \\ \alpha_{134} \\ \alpha_{124} \\ \alpha_{123} \end{pmatrix} = \begin{pmatrix} 0 \\ 0 \\ 0 \\ 1 \end{pmatrix}, \quad (12)$$

where p_1, \dots, p_4 are the external momenta, $p_5 = p_1 + p_2$, $p_6 = p_2 + p_3$ and the m_i are loop particle masses.

This approach allows us to construct quite compact expressions for the one-loop amplitudes for the processes of interest in terms of kinematical factors and scalar integrals of the form $B_0(p^2; m_1^2, m_2^2)$ and $C_0(p_1^2, p_2^2, p_5^2; m_1^2, m_2^2, m_3^2)$. For example, the total amplitude for $B_H B_H \rightarrow \gamma\gamma$ via loops of one (massless) fermion species and its KK partners is given by:

mathematical factors and scalar integrals of the form $B_0(p^2; m_1^2, m_2^2)$ and $C_0(p_1^2, p_2^2, p_5^2; m_1^2, m_2^2, m_3^2)$. For example, the total amplitude for $B_H B_H \rightarrow \gamma\gamma$ via loops of one (massless) fermion species and its KK partners is given by:

$$\begin{aligned} A_1^{(\ell)} = & -\alpha_Y \alpha_{em} Q_\ell^2 (Y_L^2 + Y_R^2) \left\{ 2 + \frac{2}{1-\eta} B_0(M_{B_H}^2; M_L^2, 0) - B_0(4M_{B_H}^2; 0, 0) - \frac{1+\eta}{1-\eta} B_0(4M_{B_H}^2; M_L^2, M_L^2) \right. \\ & + M_{B_H}^2 \left[-(1+\eta)(C_0(M_{B_H}^2, 4M_{B_H}^2, M_{B_H}^2; M_L^2, 0, 0) + C_0(M_{B_H}^2, 4M_{B_H}^2, M_{B_H}^2; 0, M_L^2, M_L^2)) \right. \\ & \left. \left. - 2C_0(M_{B_H}^2, 0, M_{B_H}^2; 0, M_L^2, M_L^2) + 4\eta C_0(0, 0, 4M_{B_H}^2; M_L^2, M_L^2, M_L^2) \right] \right\}, \quad (13) \end{aligned}$$

where α_{em} and α_Y denote the SM fine structure constant and $U(1)$ coupling constants, respectively. The charge of the fermion is Q_ℓ (in units of e), while $Y_{L,R}$ are the left- and right-handed hypercharge quantum numbers of the fermion. In the above and the following, we assume a common mass for all KK fermions M_L (i.e., we neglect any mass splittings) and we define $\eta \equiv M_L^2/M_{B_H}^2$. Similar (though more complicated) expressions hold for the amplitudes for the processes $B_H B_H \rightarrow \gamma V$ where V is a massive gauge boson (e.g., a SM Z boson or a higher KK mode such as the $B^{(1,1)}$).

tween $V\bar{\ell}\ell$ and $V\bar{\xi}\xi$ are nearly the same strength and the result is a significant cancellation between the various diagrams. However, in the case where V is identified with the $B^{(1,1)}$ KK gauge boson, the $V\bar{\ell}\ell$ couplings are loop-suppressed, while the $V\bar{\xi}\xi$ couplings are relatively large. This results in less cancellation between the various diagrams and an enhanced cross section compared to the other two processes.

In Fig. 3, we plot the annihilation cross sections for $\gamma\gamma$, $Z\gamma$ and $B^{(1,1)}\gamma$ production as a function of the LKP mass M_{B_H} . Here and in what follows, we have exchanged the compactification scale L for the LKP mass and then derived the other KK masses (M_L and $M_{B^{(1,1)}}$) in terms of M_{B_H} , using $M_L = 1.17M_{B_H}$ and $M_{B^{(1,1)}} = 1.6M_{B_H}$, but our results are not strongly dependent on these assumptions unless the mass splittings are unusually large. It is interesting to note the enhancement of the $B^{(1,1)}\gamma$ cross section compared to the $\gamma\gamma$ and $Z\gamma$ cross sections. This effect can be understood as follows. First, in the cases where V is either a photon or a Z boson, the couplings be-

A. Line Spectra

While the spectrum of the $\gamma\gamma$ line is simply a delta function at M_{B_H} , the lines arising from the process $B_H B_H \rightarrow \gamma V$ will exhibit a line with an intrinsic width, which will depend on the mass of the boson in the final state M_V ,

$$\frac{dN_\gamma^V}{dE} = \frac{4M_{B_H} M_V \Gamma_V}{f_1 f_2}, \quad (14)$$

where Γ_V is the V width and

$$f_1 \equiv \left[\tan^{-1} \left(\frac{M_V}{M_{B_H}} \right) + \tan^{-1} \left(\frac{4M_{B_H}^2 - M_V^2}{M_V \Gamma_V} \right) \right],$$

$$f_2 \equiv \left[(4M_{B_H}^2 - 4M_{B_H} E_\gamma - M_V^2)^2 + \Gamma_V^2 M_V^2 \right].$$

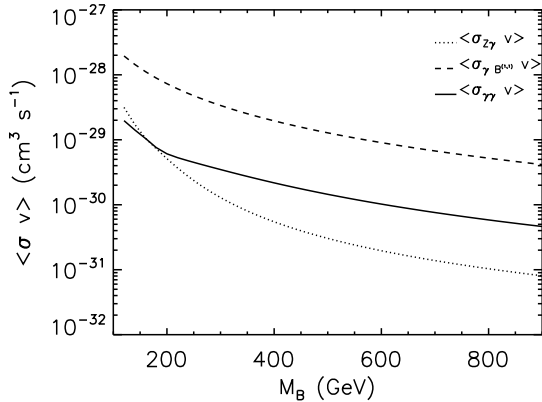


FIG. 3: Cross sections as a function of the LKP mass m_{B_H} for the three different channels $\gamma\gamma$ (solid), γZ (dotted) and $\gamma B^{(1,1)}$ (dashed).

For $B_H B_H \rightarrow Z\gamma$, we use the experimentally measured values of $M_Z \simeq 91$ GeV and $\Gamma_Z \simeq 2.5$ GeV [23]. For $B_H B_H \rightarrow B^{(1,1)}\gamma$, we have assumed the minimal mass boundary term relation $M_{B^{(1,1)}} \approx 1.6M_{B_H}$. The width of $B^{(1,1)}$ is determined by its decays into SM particles. Such interactions result entirely from boundary terms, and under the minimal assumption that they are loop-suppressed [13], we expect small coupling to the SM such that $\Gamma_{B^{(1,1)}} \approx 10^{-4}M_{B^{(1,1)}}$. Since $\Gamma_{B^{(1,1)}}$ is typically much smaller than the typical experimental energy resolutions, the resulting signals at detectors are not very sensitive to its precise value.

Generally, the larger the mass of V , the further away its corresponding line will be from the limiting value M_{B_H} . The chiral square model is interesting in this respect because the $B^{(1,1)}$ mass is large with respect to both M_Z and M_{B_H} , while still kinematically allowed. This leads to a photon distribution for the $B_H B_H \rightarrow B^{(1,1)}\gamma$ process that peaks at energies that are far below the ones associated with the $Z\gamma$ and $\gamma\gamma$ processes, which in turn makes the $B^{(1,1)}\gamma$ line clearly distinguishable from the other two lines even by current experiments, characterised by a relatively large energy resolution.

V. PROSPECTS FOR DETECTION

In order to predict the γ -ray flux from the galactic center generated by the chiral square model, we turn to the evaluation of the spectra for the $B_H B_H \rightarrow \gamma V$ processes and of the astrophysical

uncertainties related to the integration over the dark matter distribution. The differential flux of photons arising from dark matter annihilation observed in a direction making an angle ψ with the direction to the galactic center (GC) is given by

$$\frac{d\Phi_\gamma}{d\Omega dE}(\psi, E) = \frac{r_\odot \rho_\odot^2}{4\pi M_{B_H}^2} \frac{dN_\gamma}{dE} \int_{\text{l.o.s.}} \frac{ds}{r_\odot} \left[\frac{\rho[r(s, \psi)]}{\rho_\odot} \right]^2 \quad (15)$$

with

$$\frac{dN_\gamma}{dE} = \sum_f \langle \sigma v \rangle_f \frac{dN_\gamma^f}{dE}, \quad (16)$$

where we use the index f to denote the annihilation channels with one or more photons in the final state, $\langle \sigma v \rangle_f$ is the corresponding cross section and dN_γ^f/dE is the (normalized) photon spectrum per annihilation. Furthermore, $\rho(\vec{x})$, $\rho_\odot = 0.3$ GeV/cm³ and $r_\odot = 8.5$ kpc respectively denote the dark matter density at a generic location \vec{x} with respect to the GC, its value at the solar system location and the distance of the Sun from the GC. Finally, the coordinate s runs along the line of sight, which in turn makes an angle ψ with respect to the direction of the GC.

The specification of the dark matter profile is the largest source of uncertainty in the evaluation of the detectability of a dark matter annihilation signal arising from the galactic center, as it fixes the normalization of the predicted flux. The most recent high-resolution numerical simulations show that DM halos can be reasonably well fit with the Navarro Frenk and White (NFW) profile, which is often used as a benchmark for indirect searches [24]

$$\rho_{\text{NFW}}(r) = \frac{\rho_s}{\frac{r}{r_s} \left(1 + \frac{r}{r_s}\right)^2}. \quad (17)$$

However, modifications of the above profile on very small scales have been observed in the most recent simulations. In Ref. [25] it was argued that the innermost regions of DM halos are better approximated with $r^{-1.2}$ cusps, while in Ref. [26] it was found that the analytic form that provides an optimal fit to the simulated halos is the so-called ‘Einasto profile’ [27]

$$\rho(r) = \rho_0 \exp \left[-\frac{2}{\alpha} \left(\left(\frac{r}{R} \right)^\alpha - 1 \right) \right], \quad (18)$$

which is shallower than NFW at very small radii².

² The values assumed for the parameters are in this case $\alpha = 0.17$ and $R = 20$ kpc.

Model	$J(10^{-5})$
NFW	1.5×10^4
Adiabatic	4.7×10^7

TABLE I: Value of $\bar{J}(10^{-5})$ for the dark matter density profiles adopted in Fig. 4

These results have been derived in the framework of simulations containing only dark matter, not taking baryons into account, which are expected to play an important role in the dynamics of galaxies, especially on small scales. Due to dissipative processes, baryons in fact lose energy and contract, thus affecting the gravitational potential experienced by DM. In the ‘‘adiabatic compression’’ scenario [28], the baryons contraction is quasi-stationary and spherically symmetric. If one starts from an initial NFW profile, the final slope in the innermost regions is $r^{-1.5}$ [29, 30, 31, 32]. Other processes, such as the ‘‘heating’’ of the DM fluid due to gravitational interaction of baryons, may have the opposite effect on the final DM distribution, thus depleting the central cusps.

Furthermore, the presence of a super-massive black hole (BH) will inevitably affect the DM profile, especially within its gravitational radius (i.e. where the gravitational potential is dominated by the black hole itself). The growth of the BH from an initial small seed would initially lead to a large DM overdensity, or ‘spike’ [33]. Dynamical effects, and DM annihilations, will subsequently tend to destroy the spike [32, 34, 35], although in some cases significant overdensities can survive over a Hubble time. In what follows, we will show our results for two profiles: NFW, and the adiabatically contracted profile, with the same parameters as the profile labelled ‘A’ in Ref. [32].³

In order to quantify the astrophysical uncertainties related to the dark matter density profile and to separate them from the microphysics, we identify with J the dimensionless integral along the line-of-sight appearing in Eq. (15) and with \bar{J} its average value computed for a solid angle $\Delta\Omega$ cen-

tered on the GC

$$J \equiv \int_{\text{l.o.s.}} \frac{ds}{r_\odot} \left[\frac{\rho[r(s, \psi)]}{\rho_\odot} \right]^2,$$

$$\bar{J}(\Delta\Omega) = \frac{1}{\Delta\Omega} \int_{\Delta\Omega} J(\psi) d\Omega. \quad (19)$$

In Tab. I we show the values of \bar{J} for the two halo profiles adopted in Fig. 4, obtained assuming $\Delta\Omega = 10^{-5}$ sr., corresponding to the angular resolution of the HESS and Fermi LAT γ -ray experiments.

To account for the finite resolution of the detector we convolve the unfiltered ‘‘raw’’ signal $S(E)$ with a gaussian kernel $G(E, E_0)$,

$$G(E, E_0) = \frac{1}{\sqrt{2\pi}E_0\sigma} \exp\left[-\frac{(E - E_0)^2}{2\sigma^2 E_0^2}\right], \quad (20)$$

where σ is related to the detector’s relative energy resolution ξ by $\sigma = \xi/2.3$. The signal $S_M(E_0)$ measured by the detector at energy E_0 is then simply given by

$$S_M(E_0) = \int dE G(E, E_0) S(E). \quad (21)$$

We show in Fig. 4 the final predicted fluxes, from a solid angle $\Delta\Omega = 10^{-5}$ towards the galactic center, for the chiral square model with $M_{BH} = 250$ GeV and $M_{BH} = 450$ GeV and for two different choices of the DM profile. Masses of relevant states for these two mass scenarios are given in Tab. II. We show both the actual spectrum (dotted lines) and the spectrum as it would be observed by an experiment with a 10% energy resolution (solid) such as Fermi-LAT. We also show for comparison the HESS data for the point source HESS J1745-290, which is spatially coincident, within the angular resolution of HESS, with the supermassive black hole Sgr A* lying at the center of the Galaxy [36].

VI. DISCUSSION AND CONCLUSIONS

As can be easily seen from Fig. 4, the WIMP forest in the chiral square scenario is characterized by three lines. The two lines at and around M_{BH} ,

M_{BH}	L^{-1}	M_L	$M_{B^{(1,1)}}$
250	290	294	401
450	521	528	721

TABLE II: Masses of B_H , $\xi_{s,d}^{(\ell)}$ and $B^{(1,1)}$ and curvature in GeV for the two mass scenarios given in Fig. 4.

³ Note that our values of J for the NFW and ‘‘Adiabatic’’ profiles are slightly different from the values in Ref. [32], due to the fact that the NFW profile was there approximated as a simple r^{-1} power-law from the galactic center to the location of the Sun.

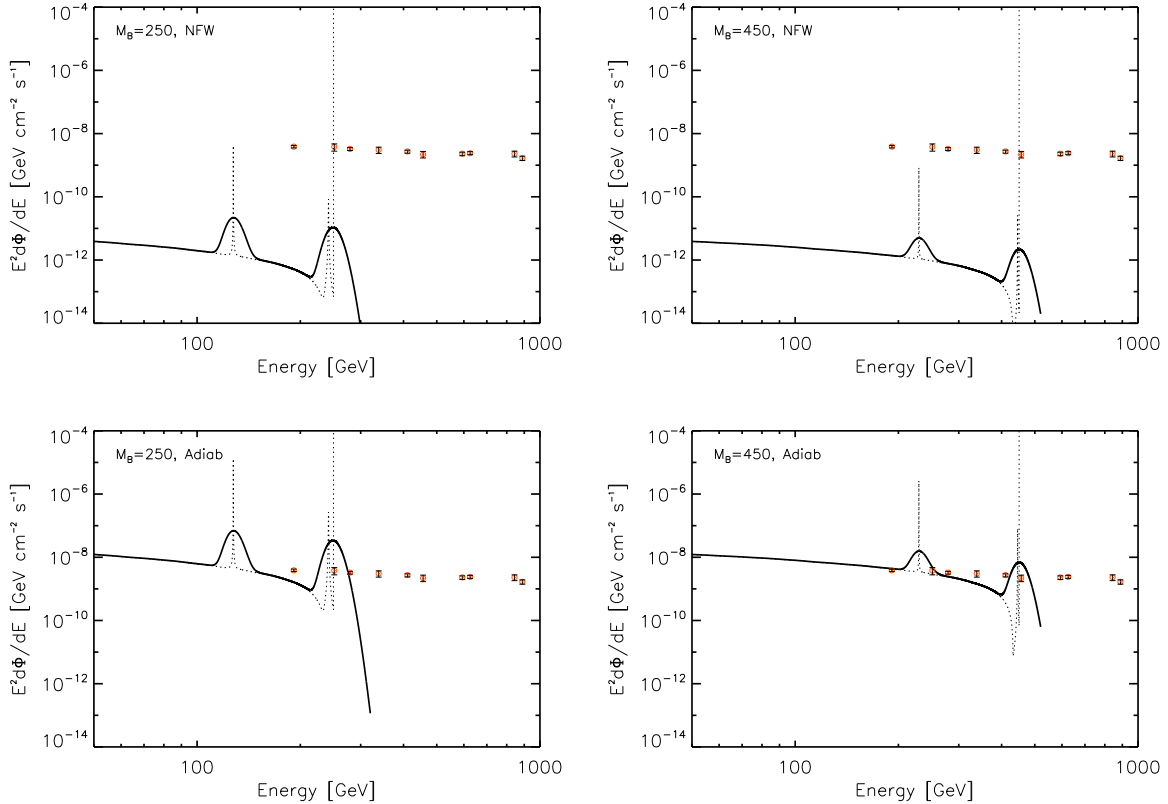


FIG. 4: Predicted fluxes, from a solid angle $\Delta\Omega = 10^{-5}$ towards the GC, for the chiral square model with $M_{B_H} = 250$ GeV (left column) and $M_{B_H} = 450$ GeV (right). We show both the actual spectrum (dotted lines) and the spectrum as it would be observed by an experiment with a 10% energy resolution (solid) like Fermi LAT. An NFW (adiabatically compressed) profile has been adopted for the lower (upper) panels. We show for reference the HESS data relative to the gamma-ray source detected at the Galactic center.

belonging respectively to the $B_H B_H \rightarrow \gamma\gamma$ and the $B_H B_H \rightarrow Z\gamma$ processes cannot be resolved by a detector whose resolution is only 10% and they appear as a single bump. On the other hand, the $B_H B_H \rightarrow B^{(1,1)}\gamma$ process is really the distinctive feature of the chiral square model, leading to a line at much lower energies that is clearly distinguishable from the other ones even by detector with only fair energy resolution. The information content of such a line can be hardly overemphasized. Since 5D Kaluza-Klein models are lacking such a feature, experimental observation of this line would not only make a strong case for Kaluza-Klein dark matter but also indicate the presence of *two* extra dimensions compactified along the lines of the chiral square model and allow a first measurement of the *size* of such extra dimensions.

Figure 4 also shows that, for a suitable choice of astrophysical and particle physics parameters (especially for an ‘optimistic’ DM profile), the anni-

hilation flux in this scenario is within the reach of current experiments. The size of the error bars in the HESS data, also suggests that the WIMP forest (an abbreviated name for the “forest of gamma-ray lines produced by WIMP annihilations”) might be realistically detected as a “double bump” in the energy spectrum. It should be kept in mind, however, that the HESS source actually exhibits a flat, feature-less, spectrum extending over two decades in energy. This means that the underlying emission probably originates from an ordinary astrophysical source, and that this source represents a foreground for a DM-induced signal.

A better strategy might consist in the analysis of the gamma-ray emission from a broader region, e.g. a cone of several degrees towards the center, or an annulus that excludes the galactic plane [37, 38]. A dedicated analysis of the various detection strategies, also containing a discussion of the prospects for detecting gamma-ray

lines with the Fermi LAT, has been recently published in Ref. [37], where the authors conclude that for robust identification, annihilation cross-sections to lines as high as $\sigma v \sim 10^{-26} \text{ cm}^3 \text{ s}^{-1}$ are required, for an NFW profile. With steeper profiles, even smaller cross sections lead to annihilation fluxes comparable with, or larger than, astrophysical backgrounds, thus becoming potentially accessible to gamma-ray telescopes. In Ref. [39], for instance, it is shown that a suitable choice of the observational window may allow to probe cross sections of order $\sigma v \sim 10^{-29} \text{ cm}^3 \text{ s}^{-1}$ for profiles steeper than $r^{-1.5}$. These results however strongly depend on the intensity and shape of astrophysical foregrounds, that the authors approximated with an analytic fit to EGRET data proposed over a decade ago in Ref. [40]. Preliminary Fermi measurements suggest that EGRET may have overestimated the flux of photons at GeV energies, therefore a word of caution is in order when estimating the prospects for detecting gamma-ray lines in this energy range.

Several other targets for indirect detection have been proposed over the years (see Refs. [1] for a discussion and references). The current understanding is that, aside from a small region of size $\mathcal{O}(1)$ degrees from the galactic center, the diffuse flux is dominated by annihilations in Galactic unresolved substructures [41, 42], while the extragalactic contribution is expected to be subdominant [43]. Alternative targets include clumps of DM (e.g. [37, 41, 42] and references therein) and mini-spikes around Intermediate Mass Black Holes [44].

In closing, gamma rays from the annihilation of dark matter are a fascinating signal that can tell us a lot about the underlying particle theory, and probe the distribution of WIMPs in the galaxy. The lines of the WIMP forest serve to measure the mass of the WIMP, detect the presence of other states in the dark sector, and perhaps even identify which theory of dark matter is responsible for a signal. While we have worked in the specific context of a six dimensional UED model, the feature itself is more general, and can be present any time two WIMPs can annihilate into a photon and another massive boson. As we enter an exciting new era of possibilities to detect WIMPs indirectly, it is important to search for multiple features in the spectrum of gamma rays.

Acknowledgments

The authors are grateful for conversations with Bogdan Dobrescu, Dan Hooper, Rakhi Mahbubani, Simona Murgia, Geraldine Servant, and especially to Eduardo Ponton, and K.C. Kong (particularly for his publicly available chiral square micrOMEGAs model files). T. Tait is grateful to the SLAC theory group for their extraordinary generosity during his many visits. Research at Argonne National Laboratory is supported in part by the Department of Energy under contract DE-AC02-06CH11357. A Vallinotto is supported by the DOE and the NASA at Fermilab.

-
- [1] G. Jungman, M. Kamionkowski and K. Griest, *Phys. Rept.* **267**, 195 (1996) [arXiv:hep-ph/9506380]; L. Bergstrom, *Rept. Prog. Phys.* **63**, 793 (2000) [arXiv:hep-ph/0002126]; G. Bertone, D. Hooper and J. Silk, *Phys. Rept.* **405** (2005) 279 [arXiv:hep-ph/0404175].
- [2] L. Bergstrom, T. Bringmann, M. Eriksson and M. Gustafsson, *Phys. Rev. Lett.* **94**, 131301 (2005) [arXiv:astro-ph/0410359]; A. Birkedal, K. T. Matchev, M. Perelstein and A. Spray, arXiv:hep-ph/0507194, J. F. Beacom, N. F. Bell and G. Bertone, *Phys. Rev. Lett.* **94** (2005) 171301 [arXiv:astro-ph/0409403].
- [3] L. Bergstrom and P. Ullio, *Nucl. Phys. B* **504**, 27 (1997) [arXiv:hep-ph/9706232]; Z. Bern, P. Gondolo and M. Perelstein, *Phys. Lett. B* **411**, 86 (1997) [arXiv:hep-ph/9706538]; P. Ullio and L. Bergstrom, *Phys. Rev. D* **57**, 1962 (1998) [arXiv:hep-ph/9707333]; L. Bergstrom, P. Ullio and J. H. Buckley, *Astropart. Phys.* **9**, 137 (1998) [arXiv:astro-ph/9712318].
- [4] B. A. Dobrescu and E. Ponton, *JHEP* **0403**, 071 (2004) [arXiv:hep-th/0401032]; G. Burdman, B. A. Dobrescu and E. Ponton, *JHEP* **0602**, 033 (2006) [arXiv:hep-ph/0506334]; G. Burdman, B. A. Dobrescu and E. Ponton, *Phys. Rev. D* **74**, 075008 (2006) [arXiv:hep-ph/0601186]; B. A. Dobrescu, K. Kong and R. Mahbubani, *JHEP* **0707**, 006 (2007).
- [5] T. Appelquist, H. C. Cheng and B. A. Dobrescu, *Phys. Rev. D* **64**, 035002 (2001) [arXiv:hep-ph/0012100].
- [6] B. A. Dobrescu, D. Hooper, K. Kong and R. Mahbubani, *JCAP* **0710**, 012 (2007) [arXiv:0706.3409 [hep-ph]].
- [7] G. Servant and T. M. P. Tait, *Nucl. Phys. B* **650**, 391 (2003) [arXiv:hep-ph/0206071];

- M. Kakizaki, S. Matsumoto, Y. Sato and M. Senami, Phys. Rev. D **71**, 123522 (2005) [arXiv:hep-ph/0502059]; M. Kakizaki, S. Matsumoto, Y. Sato and M. Senami, Nucl. Phys. B **735**, 84 (2006) [arXiv:hep-ph/0508283]; F. Burnell and G. D. Kribs, Phys. Rev. D **73**, 015001 (2006) [arXiv:hep-ph/0509118]; K. Kong and K. T. Matchev, JHEP **0601**, 038 (2006) [arXiv:hep-ph/0509119]; N. R. Shah and C. E. M. Wagner, Phys. Rev. D **74**, 104008 (2006) [arXiv:hep-ph/0608140].
- [8] H. C. Cheng, J. L. Feng and K. T. Matchev, Phys. Rev. Lett. **89**, 211301 (2002) [arXiv:hep-ph/0207125]. G. Servant and T. M. P. Tait, New J. Phys. **4**, 99 (2002) [arXiv:hep-ph/0209262].
- [9] D. Hooper and G. D. Kribs, Phys. Rev. D **67**, 055003 (2003) [arXiv:hep-ph/0208261]; G. Bertone, G. Servant and G. Sigl, Phys. Rev. D **68**, 044008 (2003) [arXiv:hep-ph/0211342]; D. Hooper and G. D. Kribs, Phys. Rev. D **70**, 115004 (2004) [arXiv:hep-ph/0406026]; T. Bringmann, JCAP **0508**, 006 (2005) [arXiv:astro-ph/0506219]; A. Barrau, P. Salati, G. Servant, F. Donato, J. Grain, D. Maurin and R. Taillet, Phys. Rev. D **72**, 063507 (2005) [arXiv:astro-ph/0506389].
- [10] L. Bergstrom, T. Bringmann, M. Eriksson and M. Gustafsson, Phys. Rev. Lett. **94**, 131301 (2005) [arXiv:astro-ph/0410359].
- [11] T. Appelquist, B. A. Dobrescu, E. Ponton and H. U. Yee, Phys. Rev. Lett. **87**, 181802 (2001) [arXiv:hep-ph/0107056].
- [12] B. A. Dobrescu and E. Poppitz, Phys. Rev. Lett. **87**, 031801 (2001) [arXiv:hep-ph/0102010].
- [13] E. Ponton and L. Wang, JHEP **0611**, 018 (2006) [arXiv:hep-ph/0512304].
- [14] H. Georgi, A. K. Grant and G. Hailu, Phys. Lett. B **506**, 207 (2001) [arXiv:hep-ph/0012379].
- [15] H. C. Cheng, K. T. Matchev and M. Schmaltz, Phys. Rev. D **66**, 036005 (2002) [arXiv:hep-ph/0204342].
- [16] M. S. Carena, T. M. P. Tait and C. E. M. Wagner, Acta Phys. Polon. B **33**, 2355 (2002) [arXiv:hep-ph/0207056].
- [17] T. Flacke, A. Menon and D. J. Phalen, arXiv:0811.1598 [hep-ph].
- [18] G. Belanger, F. Boudjema, A. Pukhov and A. Semenov, Comput. Phys. Commun. **177**, 894 (2007).
- [19] A. Pukhov, arXiv:hep-ph/0412191.
- [20] <http://home.fnal.gov/~kckong/6d/>
- [21] G. Passarino and M. J. G. Veltman, Nucl. Phys. B **160**, 151 (1979).
- [22] R. G. Stuart, Comput. Phys. Commun. **48**, 367 (1988).
- [23] C. Amsler *et al.* [Particle Data Group], Phys. Lett. B **667**, 1 (2008).
- [24] J. F. Navarro, C. S. Frenk and S. D. M. White, Astrophys. J. **462**, 563 (1996) [arXiv:astro-ph/9508025].
- [25] J. Diemand, M. Zemp, B. Moore, J. Stadel and M. Carollo, Mon. Not. Roy. Astron. Soc. **364**, 665 (2005) [arXiv:astro-ph/0504215].
- [26] J. F. Navarro *et al.*, arXiv:0810.1522 [astro-ph].
- [27] A. W. Graham, D. Merritt, B. Moore, J. Diemand and B. Terzic, Astron. J. **132**, 2685 (2006) [arXiv:astro-ph/0509417].
- [28] G. R. Blumenthal, S. M. Faber, R. Flores and J. R. Primack, Astrophys. J. **301**, 27 (1986).
- [29] J. Edsjo, M. Schelke and P. Ullio, JCAP **0409**, 004 (2004) [arXiv:astro-ph/0405414].
- [30] F. Prada, A. Klypin, J. Flix, M. Martinez and E. Simonneau, Phys. Rev. Lett. **93**, 241301 (2004) [arXiv:astro-ph/0401512].
- [31] O. Y. Gnedin, A. V. Kravtsov, A. A. Klypin and D. Nagai, Astrophys. J. **616**, 16 (2004) [arXiv:astro-ph/0406247].
- [32] G. Bertone and D. Merritt, Phys. Rev. D **72** (2005) 103502 [arXiv:astro-ph/0501555].
- [33] P. Gondolo and J. Silk, Phys. Rev. Lett. **83**, 1719 (1999) [arXiv:astro-ph/9906391].
- [34] D. Merritt, M. Milosavljevic, L. Verde and R. Jimenez, Phys. Rev. Lett. **88**, 191301 (2002) [arXiv:astro-ph/0201376].
- [35] P. Ullio, H. Zhao and M. Kamionkowski, Phys. Rev. D **64**, 043504 (2001) [arXiv:astro-ph/0101481].
- [36] F. Aharonian *et al.* [H.E.S.S. Collaboration], Phys. Rev. Lett. **97**, 221102 (2006) [Erratum-ibid. **97**, 249901 (2006)] [arXiv:astro-ph/0610509].
- [37] E. A. Baltz *et al.*, JCAP **0807** (2008) 013 [arXiv:0806.2911 [astro-ph]].
- [38] F. Stoehr, S. D. M. White, V. Springel, G. Tormen and N. Yoshida, Mon. Not. Roy. Astron. Soc. **345** (2003) 1313 [arXiv:astro-ph/0307026].
- [39] P. D. Serpico and G. Zaharijas, Astropart. Phys. **29** (2008) 380 [arXiv:0802.3245 [astro-ph]].
- [40] L. Bergstrom, P. Ullio and J. H. Buckley, Astropart. Phys. **9** (1998) 137 [arXiv:astro-ph/9712318].
- [41] L. Pieri, G. Bertone and E. Branchini, Mon. Not. Roy. Astron. Soc. **384** (2008) 1627 [arXiv:0706.2101 [astro-ph]].
- [42] V. Springel *et al.*, arXiv:0809.0894 [astro-ph].
- [43] M. Fornasa, L. Pieri, G. Bertone and E. Branchini, arXiv:0901.2921 [astro-ph].
- [44] G. Bertone, A. R. Zentner and J. Silk, Phys. Rev. D **72** (2005) 103517 [arXiv:astro-ph/0509565].